ELSEVIER

Journal of Alloys and Compounds 349 (2003) 41–48

Journal of ALLOYS AND COMPOUNDS

www.elsevier.com/locate/jallcom

Site preference and vibrational properties of $ScCu_xAl_{12-x}$

Yan-mei Kang[a,*], Nan-xian Chen[a,b]

[a] *Department of Physics, Tsinghua University, Beijing 100084, PR China*
[b] *Institute of Applied Physics, University of Science and Technology Beijing, Beijing 100083, PR China*

Received 29 January 2002; received in revised form 3 July 2002; accepted 9 July 2002

Abstract

The phase stability and site preference of Cu in $ScCu_xAl_{12-x}$ were studied based on the pair potentials obtained by the lattice inversion method. The lattice constants of $ScCu_xAl_{12-x}$ with the content x were calculated and the results are in good agreement with experiment. The properties related to lattice vibration, such as the phonon density of states, specific heat and vibrational entropy, were also evaluated. The Debye and Einstein temperatures were used to characterize the acoustic branches and optic branches, respectively. In addition, several simple mechanical properties were investigated.

Keywords: Rare earth compounds; Preferential site ordering; Crystal structure; Computer simulations

1. Introduction

In 1997, $ScCu_xAl_{12-x}$ alloys were obtained for the first time by Suski et al. [1]. These materials exist as single-phase materials for the composition range $4 \leq x \leq 6.15$. They crystallize in the tetragonal $ThMn_{12}$-type structure, which belongs to the $I4/mmm$ space group (Fig. 1). There are 26 atoms (two molecules) per unit cell. Sc atoms occupy 2*a* sites, Cu and Al atoms 8*f*, 8*j* and 8*i* positions. Experimentally, the site occupancies of the atoms in ternary compounds of rare earths are investigated mainly by X-ray powder diffraction [2–5], Mössbauer spectroscopy [6] and neutron diffraction [7–9]. The atomic distribution can also be deduced from empirical laws such as the atomic radius, atomic magnetic moment and formation enthalpy [10–12]. In this work, the preferential occupation of Cu in $ScCu_xAl_{12-x}$ alloys was evaluated by the interatomic potentials $\Phi_{Sc-Sc}(r)$, $\Phi_{Sc-Cu}(r)$, $\Phi_{Sc-Al}(r)$, $\Phi_{Cu-Cu}(r)$, $\Phi_{Cu-Al}(r)$ and $\Phi_{Al-Al}(r)$ obtained using Chen's lattice inversion method [13–16]. The results show that it is a simple and effective method for exploring the site preference in complex systems. In addition, the phonon density of states (DOS) of ternary rare earth intermetallic compounds with $ThMn_{12}$-type structure is presented with the relevant potentials for the first time. The specific heat, vibrational entropy, Einstein temperature and Debye temperature were obtained from the calculated DOS. Section 2 introduces the calculation methodology. Section 3 shows the calculated results of site preference by the energy criterion. Section 4 calculates the lattice constants. The results were compared with experimental data and the agreement is good. Sections 5 and 6 give the bulk modulus, the phonon spectra and relevant properties of $ScCu_xAl_{12-x}$, the structures of which were determined as in Section 4.

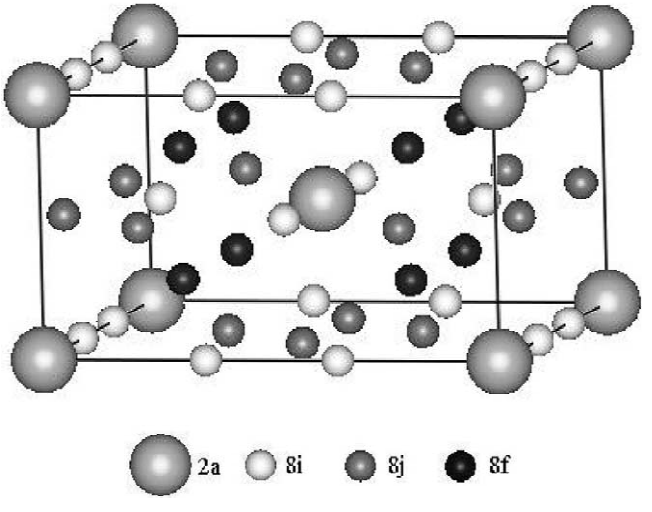

Fig. 1. Crystal structure of the $ThMn_{12}$-type compound.

*Corresponding author. Tel./fax: +86-10-6277-2783.
E-mail address: kangyanmei@tsinghua.org.cn (Y.-m. Kang).

0925-8388/02/$ – see front matter
PII: S0925-8388(02)00924-6

2. Methodology

In the early 1980s, Carlsson et al. initially proposed an inversion technique for obtaining the parameter-free pair potential [17]. However, the expression for their pair potentials includes infinite summations, each of which contains infinite terms. This made it inconvenient for analysis. In the mid-1990s, Chen et al. proposed a concise inversion theorem to avoid the above shortcomings [13–16].

2.1. Lattice inversion method

Chen's inversion theorem has been applied successfully to study the field-ion microscopy image of Fe_3Al analysis [14,18], the site preference of ternary additions in Ni_3Al and Fe_3Al [19,20], and the lattice dynamics of zinc-blend-type binary compounds [21]. For the readers' convenience, a brief introduction to this lattice inversion method is given below.

Suppose that the crystal cohesive energy can be expressed as the sum of interatomic pair potentials:

$$E(x) = \tfrac{1}{2}\sum_{n=1}^{\infty} r_0(n)\Phi[b_0(n)x] \quad (1)$$

where x is the nearest-neighbor distance, $r_0(n)$ is the coordination number of the nth neighbor, $b_0(n)x$ is the distance of the nth neighbor, $b_0(1) = 1$. The series $\{b_0(n)\}$ can be extended into a multiplicatively closed semi-group $\{b(n)\}$. In $\{b(n)\}$, for any two integers m and n, there exists a sole integer k satisfying $b(k) = b(m)b(n)$. Then Eq. (1) can be written as

$$E(x) = \tfrac{1}{2}\sum_{n=1}^{\infty} r(n)\Phi[b(n)x] \quad (2)$$

where

$$r(n) = \begin{cases} r_0(b_0^{-1}[b(n)]) & \text{if } b(n) \in \{b_0(n)\} \\ 0 & \text{if } b(n) \notin \{b_0(n)\} \end{cases} \quad (3)$$

and the pair potential from inversion can be written as

$$\Phi(x) = 2\sum_{n=1}^{\infty} I(n)E[b(n)x] \quad (4)$$

where $I(n)$ is determined by

$$\sum_{b(n)|b(k)} I(n)r\left(b^{-1}\left[\frac{b(k)}{b(n)}\right]\right) = \delta_{k1} \quad (5)$$

$I(n)$ is related only to the crystal geometrical structure, not to a concrete element category, i.e. $\{I(n)\}$ is uniquely determined by $\{r_0(n)\}$ and $\{b_0(n)\}$.

2.2. Acquisition of the cohesive energy curve

In this work, the total energy ab initio calculations (ESOCS 4.0 program provided by Materials Simulation Incorporation) were performed on the basis of an augmented spherical-wave method [22–25] within the local density functional theory. The cohesive energy is obtained from

$$E(x) = E_{\text{tot}}(x) - E_{\text{tot}}(\infty) \quad (6)$$

A series of functions $E(x)$ are calculated with various lattice constants at equal intervals of 0.1 Å. In each case, for generating the total energy, more than 80 k-points in an irreducible Brillouin zone are taken into account in a self-consistent calculation. The data are then fitted on the basis of Rose functions [26]. The obtained pair potential can generally be described by the Morse function:

$$\Phi(R) = D_0\{\exp[-2\alpha(R - R_0)] - 2\exp[-\alpha(R - R_0)]\} \quad (7)$$

where R is the distance between two atoms, and D_0, α, and R_0 are parameters. The potential parameters are listed in Table 1. To provide an intuitive impression, the calculated interatomic potentials are shown in Fig. 2.

Table 1
The potential parameters acquired by the inversion method

Potential types	R_0 (Å)	D_0 (eV)	α
Sc–Sc	3.4997	0.4465	1.1812
Cu–Cu	2.5953	0.4952	2.0266
Al–Al	3.0059	0.4232	1.4836
Sc–Cu	3.1252	0.5124	1.3686
Sc–Al	3.3507	0.4608	1.2083
Cu–Al	2.8654	0.4100	1.6117

2.3. Calculation method for DOS and thermodynamic parameters

In the harmonic approximation of the lattice dynamics, the secular equation of the lattice vibrations can be written as

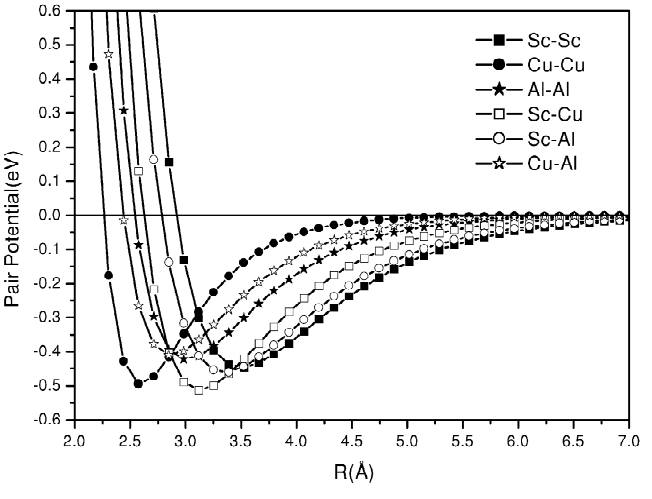

Fig. 2. Potentials of Sc–Sc, Sc–Cu, Sc–Al, Cu–Cu, Cu–Al, and Al–Al.

$$\det|D_{\alpha\beta,k\mu}(\boldsymbol{q}) - \omega^2\delta_{\alpha\beta}\delta_{k\mu}| = 0 \tag{8}$$

where ω is the angular frequency and $\boldsymbol{q}$ the wave vector. $D_{\alpha\beta}(\boldsymbol{q})$ is a dynamical matrix and its elements are written as

$$D_{\alpha\beta,k\mu} = (M_k M_\mu)^{-1/2} \sum_{R_i - R_j} \Phi_{\alpha\beta,ik,j\mu} \exp[-i\boldsymbol{q}\cdot(\boldsymbol{R}_i - \boldsymbol{R}_j)] \tag{9}$$

where $\Phi_{\alpha\beta,ik,j\mu}$ is the force constant, $\boldsymbol{R}_i$, $\boldsymbol{R}_j$ are positions in the ith and jth cell, and k, μ represent different atoms in the same cell. Using the interatomic pair potential, the force constant can be expressed as

$$\Phi_{\alpha\beta,ik,j\mu} = \begin{cases} \frac{1}{2}\left(\frac{R_\alpha R_\beta}{R^3}\Phi'_{k,\mu}(R) - \frac{R_\alpha R_\beta}{R^2}\Phi''_{k,\mu}(R) - \frac{1}{R}\Phi'_{k,\mu}(R)\delta_{\alpha\beta}\right) & \text{if } R \neq 0 \\ -\sum_{\kappa\neq\mu}\Phi_{\alpha\beta,i\mu,i\kappa} - \sum_{i\neq j}\sum_{\kappa}\Phi_{\alpha\beta,i\kappa,i\mu} & \text{if } R = 0\ (\boldsymbol{R}_i = \boldsymbol{R}_j, \boldsymbol{r}_k = \boldsymbol{r}_\mu) \end{cases} \tag{10}$$

where $R = |\boldsymbol{R}| = |\boldsymbol{R}_i - \boldsymbol{R}_j + \boldsymbol{r}_k - \boldsymbol{r}_\mu|$, $\boldsymbol{r}_k$, $\boldsymbol{r}_\mu$ are the relative positions of the different atoms in the same cell, $\Phi_{k\mu}(R)$ is the pair potential between the kth and μth atoms, and ϕ' and ϕ'' are the first and second derivative of Φ, respectively.

The phonon dispersion $\omega(\boldsymbol{q})$ is given by Eq. (8). Then the density of states $g(\omega)$ can be acquired from $\omega(\boldsymbol{q})$. The specific heat and vibrational entropy can be written as

$$C_V(T) = 3Nk_B \int_0^\infty \frac{(\hbar\omega/k_BT)^2\, e^{\hbar\omega/k_BT}}{(e^{\hbar\omega/k_BT} - 1)^2} g(\omega)\, d\omega \tag{11}$$

$$S(T) = \int_0^T \frac{C_V(T')}{T'}\, dT' \tag{12}$$

In the conventional Debye model, the Debye temperature Θ_D can be defined by $\hbar\omega_m = k_B\Theta_D$. The specific heat can be written as

$$C_V = 3Nk_B(T/\Theta_D)^3 \int_0^{\Theta_D/T} \frac{x^4\, e^x}{(e^x - 1)^2}\, dx \tag{13}$$

Similarly, in the conventional Einstein model, the Einstein temperature Θ_E can be defined by $\hbar\omega_E = k_B\Theta_E$. The specific heat can be expressed as

$$C_V = 3Nk_B(\Theta_E/T)^2 \frac{e^{\Theta_E/T}}{(e^{\Theta_E/T} - 1)^2} \tag{14}$$

where N represents the number of atoms in each cell. There are three acoustic branches and $3N-3$ optical branches. Conventionally, in the Debye model, ω_m is determined by

$$\int_0^{\omega_m} g(\omega)\, d\omega = 3N$$

that is, the integral is performed in the complete phonon density of states. In fact, the Debye model was initially proposed for approximating the low-temperature properties of materials. It essentially does not reflect the high-frequency properties of materials. Therefore, the Debye model is used for acoustic branches [27]. In this approximation, it only represents the contribution from the acoustic branch, i.e. $\int_0^{\omega_m} g(\omega)\, d\omega = 3$. In the same way, the Einstein temperature characterizes the optic branch for higher temperature; in other words, the newly defined Debye temperature Θ_{MD} is determined only by the acoustic branches and the Einstein temperature Θ_{ME} by the optic branches of the lattice vibration instead of the complete phonon spectra. In this case, the specific heats corresponding to Θ_{MD} and Θ_{ME} can be expressed as

$$C_V = 9k_B(T/\Theta_{MD})^3 \int_0^{\Theta_{MD}/T} \frac{x^4\, e^x}{(e^x - 1)^2}\, dx \tag{15}$$

and

$$C_V = (3N-3)k_B(\Theta_{ME}/T)^2 \frac{e^{\Theta_{ME}/T}}{(e^{\Theta_{ME}/T} - 1)^2} \tag{16}$$

3. Site preference in $ScCu_xAl_{12-x}$

Based on the above formulism, we may evaluate the site preference in $ScCu_xAl_{12-x}$. For convenience, let us first consider $ScAl_{12}$. Despite the structure of $ScAl_{12}$ being metastable, it can be considered as the intrinsic structure of $ScCu_xAl_{12-x}$. In the calculation the long-range interaction and coordination relations of atoms are considered. As a sample system we chose $(ScAl_{12})_{16}$ as the crystal cell with periodic boundaries in order to reduce statistical fluctuations, and we introduce relaxation governed by the interaction of pair potentials, using the conjugate gradient method with a cut-off radius of 14 Å. Within the composition range $x < 4$, the Cu atoms randomly occupy 8*i*, 8*j* and 8*f* sites. The crystal energy is the average of 100 samples and is shown in Fig. 3. This clearly shows that the cohesive energy is lowest when Al atoms at the 8*i* sites are replaced by Cu within $x < 1$. In the range $0 < x < 4$, the cohesive energy decreases when the 8*f* sites are occupied by Cu, while it increases when Cu occupies the 8*i* and 8*j* positions with increasing Cu content. In the range $1 \leq x \leq 4$ the cohesive energy is lower when Cu atoms are substituted for Al on the 8*f* sites rather than for Al on the 8*j* and 8*i* sites. This indicates that the Cu atoms preferentially occupy the 8*f* sites based on energy considerations when x is within 1 and 4. This accords with experiments on several rare earth compounds [2,7,28,29]. In the composition range $x > 4$, four Cu atoms have

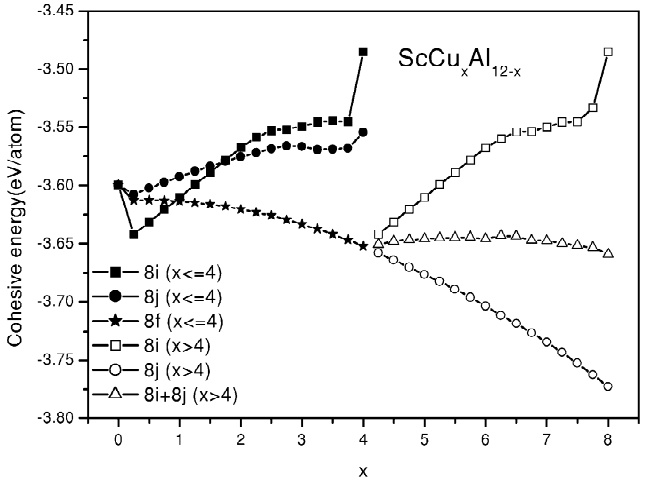

Fig. 3. Site preference of Cu in $ScCu_xAl_{12-x}$.

Table 2
Calculated cohesive energy of $ScCu_xAl_{12-x}$ after relaxation

x	0	4	4.85	5.5	6.15
Energy (eV/atom)	−3.560	−3.652	−3.674	−3.690	−3.707

already occupied the 8*f* sites based on the above analysis, so the remaining Cu atoms can only occupy the 8*i* or 8*j* sites. The calculated cohesive energy is shown in Fig. 3 when Cu atoms occupy 8*i*, 8*j* and 8*i* + 8*j* sites, respectively. The energy increases with x when the 8*i* sites are occupied by Cu atoms and remains constant when the 8*i* and 8*j* sites are occupied at the same time. The energy decreases almost linearly when the Cu atoms are substituted for Al atoms at the 8*j* sites. The results agree with experiment [29]. Therefore, when $x > 4$, the Cu atoms occupy 8*j* sites. The cohesive energies with different Cu content for $ScCu_xAl_{12-x}$ are listed in Table 2 according to the site preference.

4. The stability of $ScCu_4Al_8$

In the calculation procedure, the initial lattice constants of the metastable $ScAl_{12}$ are randomly chosen in a certain range. Under the influence of the interatomic potentials, energy minimization is performed using the conjugate gradient method. The results show that the space group is $I4/mmm$ within a tolerance of 0.001–0.1 Å. The tolerance ranges indicate the atomic derivation distance, which can be viewed as the errors in the process of determining the space group of the compound. The lattice constants after stabilization are $a = 9.243$ Å, $c = 5.252$ Å, $\alpha = \beta = \gamma = 90°$ (Table 3). The presence of a certain amount of randomness of the initial structure and the stability of the final structure illustrate that $ScAl_{12}$ has a topological invariability with respect to the stable $ScCu_4Al_8$. We applied a similar procedure to $ScCu_4Al_8$. The lattice constants after stabilization are $a = 9.075$ Å, $c = 4.956$ Å, $\alpha = \beta = \gamma = 90°$ (Table 4). The $ThMn_{12}$-type structure is retained and the lattice constants are in good agreement with experimental results after relaxation. It also demonstrates that the interatomic pair potentials are reliable for the study of the structural characteristics of materials.

According to the results for site preference, the lattice constants for $ScCu_xAl_{12-x}$ ($x \geq 4$) were calculated when the 8*j* sites are randomly occupied by Cu atoms besides the four Cu atoms occupying the 8*f* sites. The calculated results are the average of 100 samples and are shown in Table 5 together with those for $ScAl_{12}$ and the experimental data. From Table 5, one can see that our results for $ScCu_xAl_{12-x}$ ($x = 4$, 4.85, 5.5, 6.15) are in agreement with experiment. The calculated lattice constants are smaller than those of $ScAl_{12}$. The largest deviation of a is 4.84%, while that of c is 1.02%. The calculated a parameter is larger than the experimental value, while c is smaller. The error can be explained by the fact that the structures of these single-phase materials with $ThMn_{12}$-type structure display a slight orthorhombic distortion [1]. In addition, it

Table 3
Crystal constants of $ScAl_{12}$

Initial states			Final states		
a, b, c (Å)	α, β, γ (deg)	Space group	a, b, c (Å)	α, β, γ (deg)	Space group
2.5, 2.5, 1.25	90, 90, 90	$I4/mmm$	9.243, 9.243, 5.252	90, 90, 90	$I4/mmm$
18, 18, 10	90, 90, 90	$I4/mmm$	9.243, 9.243, 5.252	90, 90, 90	$I4/mmm$
9, 9, 5	80, 70, 130	$P\bar{1}$	9.243, 9.243, 5.252	90, 90, 90	$I4/mmm$
2.5, 2.5, 1.25	50, 50, 50	$C2/m$	9.243, 9.243, 5.252	90, 90, 90	$I4/mmm$
15, 15, 7.5	110, 90, 80	$P\bar{1}$	9.243, 9.243, 5.252	90, 90, 90	$I4/mmm$
3, 3, 4	120, 80, 70	$P\bar{1}$	9.243, 9.243, 5.252	90, 90, 90	$I4/mmm$
16, 9.5, 10	70, 80, 110	$P\bar{1}$	9.243, 9.243, 5.252	90, 90, 90	$I4/mmm$
3, 12, 7	80, 80, 70	$P\bar{1}$	9.243, 9.243, 5.252	90, 90, 90	$I4/mmm$
16, 6.5, 4	70, 70, 70	$P\bar{1}$	9.243, 9.243, 5.252	90, 90, 90	$I4/mmm$
3, 4, 10	80, 80, 65	$P\bar{1}$	9.243, 9.243, 5.252	90, 90, 90	$I4/mmm$
14, 15, 8	80, 95, 130	$P\bar{1}$	9.243, 9.243, 5.252	90, 90, 90	$I4/mmm$
20, 20, 20	75, 50, 85	$C2/m$	9.340, 9.254, 15.384	25.5, 63.4, 60.5	$C2/m$

Table 4
Crystal constants of $ScCu_4Al_8$

Initial states			Final states		
a, *b*, *c* (Å)	*α*, *β*, *γ* (deg)	Space group	*a*, *b*, *c* (Å)	*α*, *β*, *γ* (deg)	Space group
2.5, 2.5, 1.25	90, 90, 90	*I*4/*mmm*	9.075, 9.075, 4.956	90, 90, 90	*I*4/*mmm*
18, 18, 10	90, 90, 90	*I*4/*mmm*	9.075, 9.075, 4.956	90, 90, 90	*I*4/*mmm*
9, 9, 5	80, 70, 130	$P\bar{1}$	9.075, 9.075, 4.956	90, 90, 90	*I*4/*mmm*
2.5, 2.5, 1.25	50, 50, 50	*C*2/*m*	9.075, 9.075, 4.956	90, 90, 90	*I*4/*mmm*
15, 15, 7.5	120, 90, 70	$P\bar{1}$	9.075, 9.075, 4.956	90, 90, 90	*I*4/*mmm*
3, 3, 4	140, 80, 70	$P\bar{1}$	9.075, 9.075, 4.956	90, 90, 90	*I*4/*mmm*
16, 9.5, 10	70, 80, 110	$P\bar{1}$	9.075, 9.075, 4.956	90, 90, 90	*I*4/*mmm*
3, 12, 7	80, 80, 70	$P\bar{1}$	9.075, 9.075, 4.956	90, 90, 90	*I*4/*mmm*
16, 6, 4	70, 70, 70	$P\bar{1}$	9.075, 9.075, 4.956	90, 90, 90	*I*4/*mmm*
3, 4, 10	80, 80, 65	$P\bar{1}$	9.075, 9.075, 4.956	90, 90, 90	*I*4/*mmm*
14, 15, 8	80, 95, 130	$P\bar{1}$	9.075, 9.075, 4.956	90, 90, 90	*I*4/*mmm*
20, 20, 20	55, 55, 50	*C*2/*m*	15.281, 16.916, 13.087	47.4, 62.2, 48.5	$P\bar{1}$

can be seen from Fig. 3 that, when the content of Cu is small, the cohesive energy is lowest when the 8*i* sites are occupied by Cu, which may suggest that the 8*f* sites are the majority sites for Cu, but a small proportion of 8*i* or 8*j* sites are also occupied by Cu. This was proposed in Refs. [7,28] for experiments with rare earth compounds. In our calculations, the structure of $ScCu_xAl_{12-x}$ is assumed to be an ideal $ThMn_{12}$-type structure. This assumption may result in a deviation of the calculations from experiment.

5. Elastic properties of $ScCu_xAl_{12-x}$

Generally, the mechanical properties of these compounds can hardly be measured experimentally because of their brittleness. It requires a huge computer capacity to calculate them by an ab initio method due to their complex structure, even for the simplest mechanical properties. In this work we evaluated the elastic constants and the bulk moduli of $ScCu_xAl_{12-x}$ ($x = 4$, 4.85, 5.5, 6.15) from pair potentials. The results are listed in Table 6.

From Table 6, one can see that the components of the elastic modulus increase with the Cu content and the bulk moduli also increase almost linearly for $ScCu_xAl_{12-x}$ (Fig. 4).

Table 5
Comparison between the calculated and experimental lattice parameters [1] *a* and *c* for $ScCu_xAl_{12-x}$

x	*a*			*c*		
	Calc. (Å)	Exp. (Å)	Err. (%)	Calc. (Å)	Exp. (Å)	Err. (%)
0	9.243	–	–	5.252	–	–
4.0	9.075	8.656	4.84	4.956	5.000	0.88
4.85	8.990	8.642	4.03	4.935	4.986	1.02
5.5	8.927	8.612	3.66	4.920	4.966	0.93
6.15	8.863	8.583	3.26	4.906	4.952	0.93

Table 6
Elastic constants C_{ij} and bulk moduli for $ScCu_xAl_{12-x}$

Material	Elastic constants, C_{ij} (GPa)						Bulk modulus (GPa)
	C_{11}	C_{12}	C_{13}	C_{33}	C_{44}	C_{66}	
$ScCu_4Al_8$	307	61	92	300	74	54	155.6
$ScCu_{4.85}Al_{7.15}$	320	67	97	316	78	56	163.5
$ScCu_{5.5}Al_{6.5}$	330	71	100	329	82	57	169.7
$ScCu_{6.15}Al_{5.85}$	342	77	103	342	87	59	176.6

6. Phonon density of states of $ScCu_4Al_8$

It can be inferred from the above calculations that the site preference and lattice constants of $ScCu_xAl_{12-x}$ evaluated using the interatomic pair potentials agree well with experiment, which demonstrates that the potentials are reliable. Therefore, these potentials can be applied to calculate the lattice dynamic properties of $ScCu_4Al_8$.

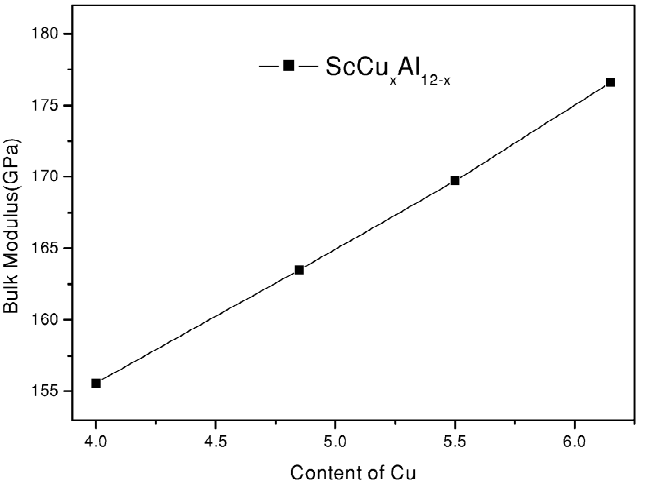

Fig. 4. Bulk modulus of $ScCu_xAl_{12-x}$.

6.1. Calculated results of phonon density of states for $ScCu_4Al_8$

In this subsection, we calculate the phonon density of states about $ScCu_4Al_8$ in the crystal cell $ScAl_{12}$ including 26 atoms. Fig. 5 shows the results of considering the contribution to the DOS of distinct atoms, including Al atoms at different crystalline sites. It can be seen that the highest frequency of $ScCu_4Al_8$ is 12.90 THz and there are four apexes around 4.2, 6.2, 7.9 and 10.0 THz, respectively. For two localized modes the frequencies are higher than 10.5 THz. The ratio of the modes excited by Sc, Cu, 8*i* Al, and 8*j* Al is 1:4:4:4 in the total frequency range. However, Sc only contributes to the modes below 7 THz. In the range 0–4.9 THz, the largest contribution is made by Cu, while in the range 5–8.5 THz, that of Al at the 8*i* sites is larger than that of the others, and the contribution of Cu is not different from that of Al at the 8*j* sites. Between 8.5 and 10.5 THz, the modes excited by Al at the 8*i* and 8*j* sites, almost equal, are much larger than those excited by Cu atoms. It should be noted that, in the higher frequency range 10.5–12.9 THz, the modes are mostly caused by 8*j* Al, and the ratio of the contribution from Cu, 8*i* Al and 8*j* Al is approximately 4:1:22.

One can analyze qualitatively the localized modes from interaction potentials by only considering the nearest neighbors in Fig. 2. The distances between the 8*j* Al atom and the nearest four Cu atoms, two 8*j* Al, two 8*i* Al and eight Sc atoms are 2.60, 2.77, 2.78 and 3.16 Å, respectively. From Fig. 6 it can be seen that Cu reacts more strongly with the nearest neighbor 8*j* Al atoms than with the 8*i* Al atoms. We may assume that the Cu atom is motionless due to its large mass relative to Al. Then the 8*j* Al atom, restricted by Cu in the Cu–Al potential well, with light mass shows local modes and corresponds to higher transverse frequency.

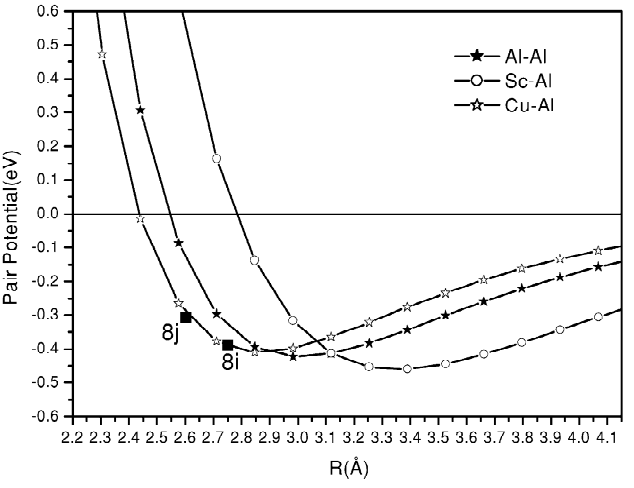

Fig. 6. Enlarged diagram for part of Fig. 2 with $2.2 \leq x \leq 4.15$ Å.

6.2. Specific heat, vibrational entropy, Debye temperature and Einstein temperature of $ScCu_4Al_8$

The specific heat $C_V(T)$, the vibrational entropy $S(T)$, the Debye temperature $\Theta_D(T)$, $\Theta_{MD}(T)$, and the Einstein temperature $\Theta_E(T)$, $\Theta_{ME}(T)$ of $ScCu_4Al_8$ can be calculated based on Eqs. (11)–(16). The results are shown in Figs. 7–10, respectively. It can be observed from Figs. 7 and 8 that the specific heat and vibrational entropy are mainly contributed from acoustic phonons at lower temperature and by optical phonons at higher temperature. Figs. 9 and 10 give the Debye temperature and Einstein temperature of $ScCu_4Al_8$. The Debye temperature at near 0 K and the Einstein temperature at about 500 K are indicated in the figures. Conventionally, both the Debye temperature and the Einstein temperature are obtained from global phonon spectra, and the former is always higher than the latter. In

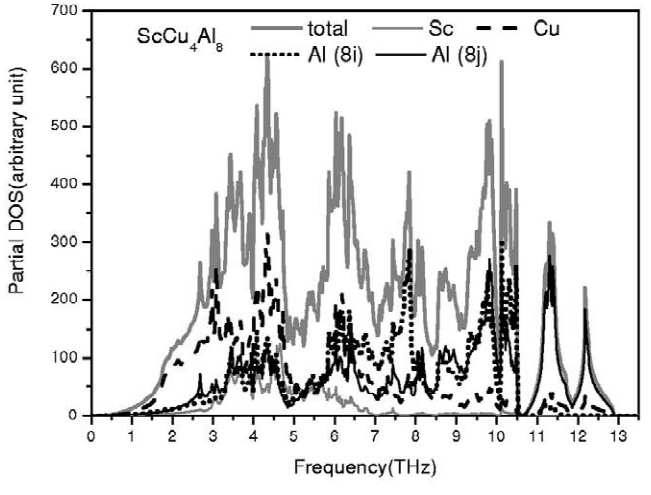

Fig. 5. Phonon density of states of $ScCu_4Al_8$.

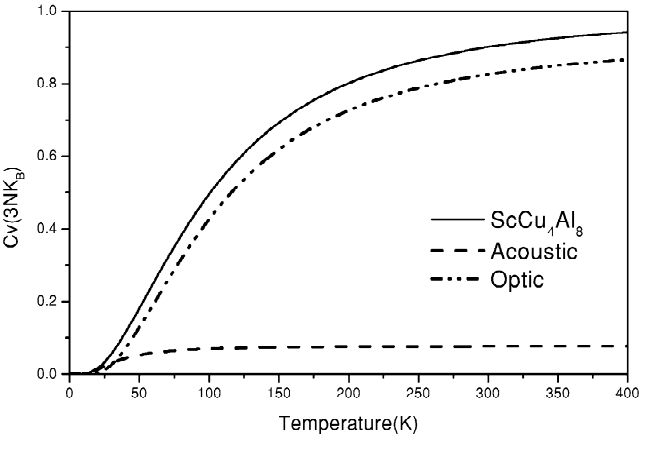

Fig. 7. Specific heat of $ScCu_4Al_8$.

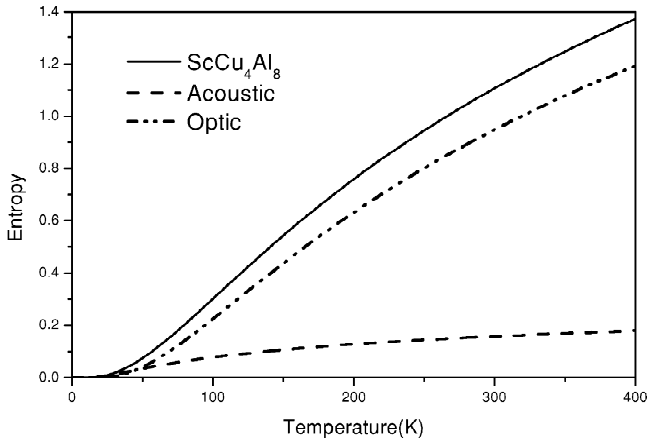

Fig. 8. Vibrational entropy of $ScCu_4Al_8$.

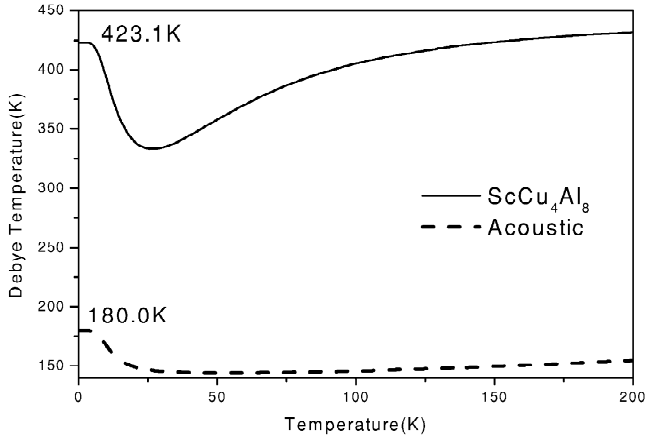

Fig. 9. Debye temperature of $ScCu_4Al_8$.

this paper, the Debye temperature and Einstein temperature characterize the lattice vibration acoustic branches and optical branches, respectively, i.e. the former is calculated only from acoustic phonons and the latter only from optical phonons. The calculated results ensure the Einstein temperature is higher than the Debye temperature.

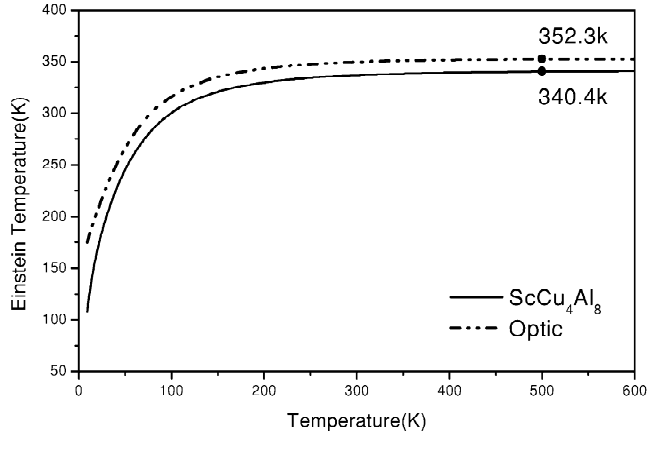

Fig. 10. Einstein temperature of $ScCu_4Al_8$.

7. Conclusion and discussion

This research applies the lattice inversion method to obtain the interatomic potentials related to rare earth compounds based on first principle calculations, which does not rely on experimental data. The site occupancies were calculated according to these potential parameters. It shows that the cohesive energy of $ScCu_4Al_8$ is much lower than that of $ScAl_{12}$ when the Cu atoms occupy all 8*f* sites. This can explain the existence of stable $ScCu_xAl_{12-x}$ phases when x is equal to or slightly larger than 4.0. The calculated lattice constants for $ScCu_xAl_{12-x}$ agree with the experimental data within a relative error of about 4%. In addition, we have also utilized the same potential parameters to evaluate the phonon density of states of $ScCu_4Al_8$, and obtained its vibrational entropy, Debye temperature and Einstein temperature. This provides some information on the vibrational properties of rare earth compounds, which are difficult to calculate and measure due to the low symmetry of the complex structure and the necessity of involving many parameters in other approaches. On the other hand, with the simplified calculation model employed in this research, it is difficult to solve problems such as the solubility and occupation fraction, because it only includes the energy and other factors and does not contain, for example, the temperature.

Acknowledgements

This work was supported in part by the National Nature Science Foundation of China (No. 59971006) and in part by the National Advanced Materials Committee of China and Special Funds for Major State Basic Research of China (Nos. G2000067101 and G2000067106).

References

[1] W. Suski, T. Cichorek, K. Wochowski, D. Badurski, B.Yu. Kotur, O.J. Bodak, Physica B 230–232 (1997) 324.
[2] I. Felner, I. Nowik, J. Phys. Chem. Solids 40 (1979) 1035.
[3] K. Ohashi, Y. Tawara, R. Osugi, M. Shimao, J. Appl. Phys. 64 (1988) 5714.
[4] K.H.J. Buschow, J. Appl. Phys. 63 (1988) 3130.
[5] Ph. Oleinek, W. Kockelmann, K.H. Müller, M. Loewenhaupt, L. Schultz, J. Alloys Comp. 281 (1998) 306.
[6] A. Krimmel, A. Loidl, C. Geibel, F. Steglich, G.J. Mcintyre, J. Magn. Magn. Mater. 103 (1992) 73.
[7] O. Moze, R.M. Ibberson, R. Caciuffo, K.H.J. Buschow, J. Less-Common Met. 166 (1990) 329.
[8] Y.C. Yang, B. Kebe, W.J. James, J. Deportes, W. Yelon, J. Appl. Phys. 52 (1981) 2077.
[9] R.B. Helmholdt, J.J.M. Vleggaar, K.H.J. Buschow, J. Less-Common Met. 138 (1988) L11.
[10] L.X. Liao, Z. Altountian, D.H. Ryan, Phys. Rev. B 47 (1993) 11230.
[11] Y.C. Chuang, C.H. Wu, Y.C. Chang, J. Less-Common Met. 84 (1982) 201.
[12] Er. Girt, Z. Altounian, Phys. Rev. B 57 (1998) 5711.

[13] N.X. Chen, Phys. Rev. Lett. 64 (1990) 1193.
[14] N.X. Chen, X.J. Ge, W.Q. Zhang, F.W. Zhu, Phys. Rev. B 57 (1998) 14203.
[15] N.X. Chen, Z.D. Chen, Y.C. Wei, Phys. Rev. E 55 (1997) R5.
[16] W.Q. Zhang, Q. Xie, X.J. Ge, N.X. Chen, J. Appl. Phys. 82 (1997) 578.
[17] A.E. Carlsson, C.D. Gelatt, H. Ehrenreich, Philos. Mag. A 41 (1980) 241.
[18] X.J. Ge, N.X. Chen, J. Appl. Phys. 85 (1999) 3488.
[19] J. Shen, Y. Wang, N.X. Chen, Y. Wu, Prog. Natural Sci. 10 (2000) 457.
[20] X.D. Ni, N.X. Chen, J. Shen, J. Mater. Res. 16 (2001) 344.
[21] Y. Liu, N.X. Chen, Y.M. Kang, Mod. Phys. Lett. B 16 (2002) 187.
[22] A.R. Williams, J. Kuebler, J.R. Gelatt, Phys. Rev. B 19 (1979) 6094.
[23] V.L. Moruzzi, C.B. Sommers, Calculated Electronic Properties of Ordered Alloys, World Scientific, Singapore, 1995.
[24] H.J. Monkhorst, J.D. Pack, Phys. Rev. B 13 (1976) 5188.
[25] D.G. Anderson, J. Assoc. Comput. Machinery 12 (1965) 547.
[26] J.M. Rose, J.R. Smith, F. Guinea, J. Ferrante, Phys. Rev. B 29 (1984) 2963.
[27] G.D. Mukherjee, C. Bansal, A. Chatterjee, Phys. Rev. Lett. 76 (1996) 1876.
[28] I. Felner, I. Nowik, J. Phys. Chem. Solids 39 (1978) 951.
[29] W. Suski, in: K.A. Gschneidner Jr., L. Eyring (Eds.), Handbook on the Physics and Chemistry of Rare Earths, Vol. 22, Elsevier, Amsterdam, 1996, p. 162, Chapter 149.